A Receptor-interacting Protein 1 (RIP1)-independent Necrotic Death under the Control of Protein Phosphatase PP2A That Involves the Reorganization of Actin Cytoskeleton and the Action of Cofilin-1

Andrea Tomasella, Anne Blangy, Claudio Brancolini

THE JOURNAL OF BIOLOGICAL CHEMISTRY VOL. 289, NO. 37, pp. 25699–25710, September 12, 2014

A Receptor-interacting Protein 1 (RIP1)-independent Necrotic Death under the Control of Protein Phosphatase PP2A That Involves the Reorganization of Actin Cytoskeleton and the Action of Cofilin-1*

Received for publication, April 18, 2014, and in revised form, July 28, 2014 Published, JBC Papers in Press, August 5, 2014, DOI 10.1074/jbc.M114.575134

Andrea Tomasella[‡1], **Anne Blangy**[§], **and Claudio Brancolini**[‡2]

From the [‡]*Dipartimento di Scienze Mediche e Biologiche Università degli Studi di Udine, P.le Kolbe 4–33100 Udine, Italy and* [§]*CNRS UMR 5237 CRBM Montpellier University 1919 Route de Mende, 34293 Montpellier Cedex 5, France*

Background: Regulation of necrosis is incompletely understood.
Results: PP2A by controlling actin cytoskeleton, also through Cofilin-1 dephosphorylation, influences a RIP1-independent necrotic signaling pathway in glioblastoma cells.
Conclusion: By comparing two different necrotic triggers we define distinct necrotic players and signaling pathways.
Significance: Understanding necrosis is fundamental to comprehend different diseases characterized by dysregulated cell loss and to alternatively kill neoplastic cells.

Cell death by necrosis is emerging not merely as a passive phenomenon but as a cell-regulated process. Here, by using different necrotic triggers, we prove the existence of two distinct necrotic pathways. The mitochondrial reactive oxygen species generator 2,3-dimethoxy-1,4-naphthoquinone elicits necrosis characterized by the involvement of RIP1 and Drp1. However, G5, a non-selective isopeptidase inhibitor, triggers a distinct necrotic pathway that depends on the protein phosphatase PP2A and the actin cytoskeleton. PP2A catalytic subunit is stabilized by G5 treatment, and its activity is increased. Furthermore, PP2Ac accumulates into the cytoplasm during necrosis similarly to HMGB1. We have also defined in the actin-binding protein cofilin-1 a link between PP2A, actin cytoskeleton, and necrotic death. Cofilin-1-severing/depolymerization activity is negatively regulated by phosphorylation of serine 3. PP2A contributes to the dephosphorylation of serine 3 elicited by G5. Finally, a cofilin mutant that mimics phosphorylated Ser-3 can partially rescue necrosis in response to G5.

Cell death by necrosis is characterized by organelle swelling and plasma membrane rupture, with the consequent release of cellular components in the microenvironment and the activation of the inflammatory response (1). Until recently necrosis was considered a passive accidental type of cell death generally observed in the presence of severe cellular stress/damage. More recently, data have been accumulated pointing to the existence of a regulated necrotic response, with dedicated genes and signaling pathways (2).

TNF-α (tumor necrosis factor) has been helpful in discovering the cellular components controlling a regulated version of necrotic death. Under particular circumstances this cytokine can trigger necrosis (3). TNF-α can stimulate the assembling of the necrosome, a signaling complex that includes the kinases RIP1,[3] R1P3, and MLKL (mixed lineage kinase domain-like) (4–7). This complex is regulated by phosphorylation, acetylation, and ubiquitination (5, 8). Necrosome-elicited death response has been defined as necroptosis, and the RIP1 inhibitor necrostatin has been instrumental in unveiling the contribution of necroptosis under different death circumstances (9).

Mitochondrial dysfunctions also mark necrosis. It was proposed that the necrosome could influence mitochondrial shape and function through the modulation of Drp1, a GTPase that controls mitochondrial fission. The mitochondrial protein PGAM5 (phosphoglycerate mutase 5), which is under the control of MLKL, could act as a downstream effector of the necroptotic signaling by dephosphorylating and thus activating Drp1 (10). This model is debated, and recently the contribution of Drp1 to necroptosis has been questioned (11, 12).

Although some hints have accumulated on cytokine- and pathogen-induced necrosis, other varieties, engaged by cellular stresses, triggered by physical agents or chemicals are still obscure (2). In addition to elements of the necroptotic pathway, further players could be involved in the stress-induced necrotic response. Lysosomal proteases released into the cytosol after lysosomal membrane permeabilization (13) and calpains, proteolytic enzymes activated by increase of Ca^{2+}, have been proposed as necrotic regulators (14, 15). In particular, the poly-(ADP-ribose) polymerase 1 (PARP-1) and cyclophilin D (CypD) have been linked in some studies to RIP1 in models of oxidative stress-induced necrosis (16, 17).

It has been proposed that the phosphoglycerate mutase 5 (PGAM5)/Drp1 axis could represent a convergent node for dif-

* This work was supported by Associazione Italiana per la Ricerca sul Cancro (IG-10437) and FIRB (Progetto RBAP11S8C3_002) (to C. B.)
[1] Recipient of a fellowship from Associazione Italiana per la Ricerca sul Cancro.
[2] To whom correspondence should be addressed. Tel.: 39-0432-494382; Fax: 39-0432-494301: E-mail: claudio.brancolini@uniud.it.

[3] The abbreviations used are: RIP1, receptor-interacting protein 1; MLKL, mixed lineage kinase-like; PP2A, protein phosphatase 2A; Nec-1, necrostatin-1; DMNQ, 2,3-dimethoxy-1,4-naphthoquinone; DiFMUP, 6,8-difluoro-4-methylumbelliferyl phosphate; TRITC, tetramethylrhodamine isothiocyanate; NSA, necrosulfonamide; Boc-fmk, butoxycarbonyl-fluoromethyl ketone; Smac, second mitochondria-derived activator of caspases.

ferent necrotic pathways (10). To clarify whether or not multiple necrotic pathways exist, we have compared the necrotic responses elicited by two different chemical stresses. Our studies indicate the existence of different necrotic pathways and identify in the protein phosphatase 2A (PP2A)-cofilin-actin axis a new regulator of a specific form of necrotic death.

EXPERIMENTAL PROCEDURES

Cell Culture, Cell Death, Retroviral Infection, and siRNA—U87MG, U-118MG, HT29, and IMR90-E1A/Bcl2/C9DN cells were grown in DMEM supplemented with 10% FBS, penicillin (100 units/ml), glutamine (2 mmol/liter), and streptomycin (100 μg/ml) at 37 °C in 5% CO_2 atmosphere. U87MG cells expressing Bcl-xL, Drp1 K38A, GFP, Cofilin constructs, and myristoylated Akt were generated by retroviral infection (18). In all trypan blue exclusion assays, at least 400 cells from three independent samples were counted. RNA oligos for interference (RNAi) were purchased from Invitrogen, Dharmacon, and Qiagen. Cells were transfected 24 h after plating by adding the Opti-MEM medium containing Lipofectamine 2000 (Invitrogen) plus RNAi oligos.

Reagents and Antibodies—The following chemicals were used: LY (LY294002; LC Laboratories), BOC-D(OMe)-fmk (Imgenex), bortezomib (LC Laboratories), necrostatin-1 (Nec-1) (Enzo Life Sciences), cytochalasin D, cucurbitacin E, 2,3-dimethoxy-1,4-naphthoquinone (DMNQ), Mdivi-1, biotinylated concanavalin A, and DMSO (Sigma), MitoTracker Red/CMXRos, 6,8-difluoro-4-methylumbelliferyl phosphate (DiFMUP), streptavidin-FITC, phalloidin-TRITC (Invitrogen/Molecular Probes), okadaic acid (Enzo Life Sciences), and necrosulfonamide (NSA) (Merck Millipore). Primary antibodies were anti-FLAG and anti-actin (Sigma), anti-nucleoporin p62, anti-Ran (RAS-related nuclear protein), anti-Bcl-xL, anti-Drp1 (DLP1) (BD Biosciences), anti-JNK Thr(P)-183/Tyr-185, anti-JNK, anti-p38, anti-pp38, anti-Erk, anti-pErk, anti-Akt, anti-Akt p473, anti-Akt p308 (Cell Signaling), anti-F1-ATP synthase, anti-cofilin-1, anti-pCofilin-1 (Santa Cruz Biotechnologies), anti-Smac/DIABLO (19), anti-PP2A/C subunit, anti-PP2A/A subunit (Upstate Biotechnology, Lake Placid, NY), and anti-HMGB1 (AbCam, Cambridge, UK). Secondary anti-mouse and anti-rabbit antibodies were Alexa Fluor 488- and Alexa Fluor 546-conjugated (Invitrogen).

Western Blotting—Cell lysates after SDS/PAGE were transferred to a 0.2-μm nitrocellulose membrane and incubated with the specific primary antibodies. For primary antibody stripping, blots were incubated for 30 min at 60 °C in stripping solution (62.5 mM Tris-HCl, pH 6.8, 2% SDS, 100 mM β-mercaptoethanol). Quantitative densitometric analysis of the immunoblots was performed by ChemiDoc software (Bio-Rad).

Phosphatase Assay—Cells were lysed directly in Petri dishes with lysis buffer (50 mM Tris-HCl, pH 8.0, 100 mM NaCl, 2 mM EDTA, and 1% (v/v) Igepal CA-630, PMSF, and a protease inhibitor mixture (Sigma). Whole cell lysates were incubated with anti-PP2Ac antibody (ON). After incubation with protein A beads the immunocomplexes were washed four times with lysis buffer. Beads were resuspended in phosphatase assay buffer (50 mM Tris-HCl, pH 7.0, and 0.1 mM $CaCl_2$), incubated for 30 min at 37 °C with or without okadaic acid 100 nM in presence of 1 mM $NiCl_2$ and 0.125 mg/ml BSA, and then analyzed by fluorimetric assay using DiFMUP substrate as described (20). Immunocomplexes were recollected after the fluorimetric assay and next resolved in SDS/PAGE electrophoresis and immunoblotted.

Immunofluorescence Microscopy—Mitochondria were labeled *in vivo* for 1 h with 25 nmol/liter MitoTracker Red. Cells were fixed with 3% paraformaldehyde and permeabilized with 0.5% Triton X-100 and incubated with the primary antibody, phalloidin-TRITC. After washes, coverslips were incubated with the relative secondary antibodies. Cells were imaged with a Leica confocal scanner SP equipped with a 488 λ Ar laser and a 543–633 λ HeNe laser. The image analysis was performed using the MetaMorph 6.04 software. Cell images for deconvolution were taken using the Leica AF6000 LX microscope. Deconvolution software was used for image deconvolution and three-dimensional view reconstruction.

RNA Extraction and Quantitative Real-time-PCR—Cells were lysed using TRI-REAGENT (Molecular Research Center). 1.0 μg of total RNA was retro-transcribed by using 100 units of Moloney murine leukemia virus reverse transcriptase (Invitrogen). Quantitative real-time-PCRs were performed using the Bio-Rad CFX96 and SYBR Green technology. Data were analyzed by a comparative threshold cycle using hypoxanthine-guanine phosphoribosyltransferase and β-actin as normalizer genes. All reactions were done in triplicate.

Statistical Analysis—Results are expressed as the means ± S.D. Student's *t* test was performed with Excel software. *p* values are represented as: *, $p < 0.05$; **, $p < 0.01$; ***, $p < 0.005$. Data of the spreading area were analyzed using Non-parametric Mann-Whitney test (Prism GraphPad Software); ***, $p < 0.0001$.

RESULTS

Characterization of Necrosis as Induced by the Non-selective Isopeptidase Inhibitor G5 and the Redox Cycling Quinone, DMNQ—To explore the existence of different necrotic signaling pathways, we used two different chemical stressors: the isopeptidases inhibitor G5, an inducer of alterations in cell adhesion and actin cytoskeleton (18, 21, 22), and DMNQ, a generator of reactive oxygen species at mitochondrial level (23).

As the cellular model to study necrosis we selected U87MG glioblastoma cells because of their intrinsic resistance to apoptosis and the tendency to die by necrosis (18). In addition, we overexpressed Bcl-xL to further suppress apoptosis.

Cells were treated with escalating doses of G5 or DMNQ, and cell death was scored by a trypan blue assay (Fig. 1*A*). In general 5 μM G5 and 20 μM DMNQ were employed for the subsequent studies. Contrary to bortezomib, G5- or DMNQ-induced cell death was unaffected by caspase inhibitors (Fig. 1*B*).

Next we evaluated the mitochondrial morphology using MitoTracker in relation to mitochondrial outer membrane permeabilization. As a marker of mitochondrial outer membrane permeabilization, we explored Smac localization. Both necrotic stimuli induced a dramatic mitochondrial fragmentation (Fig. 1*C*), with the quantitative analysis reported in Fig. 1*D*. Smac was usually retained in the mitochondria, thus proving the absence of mitochondrial outer membrane permeabilization (Fig. 1*E*). Curiously in the case of DMNQ a fraction of cells

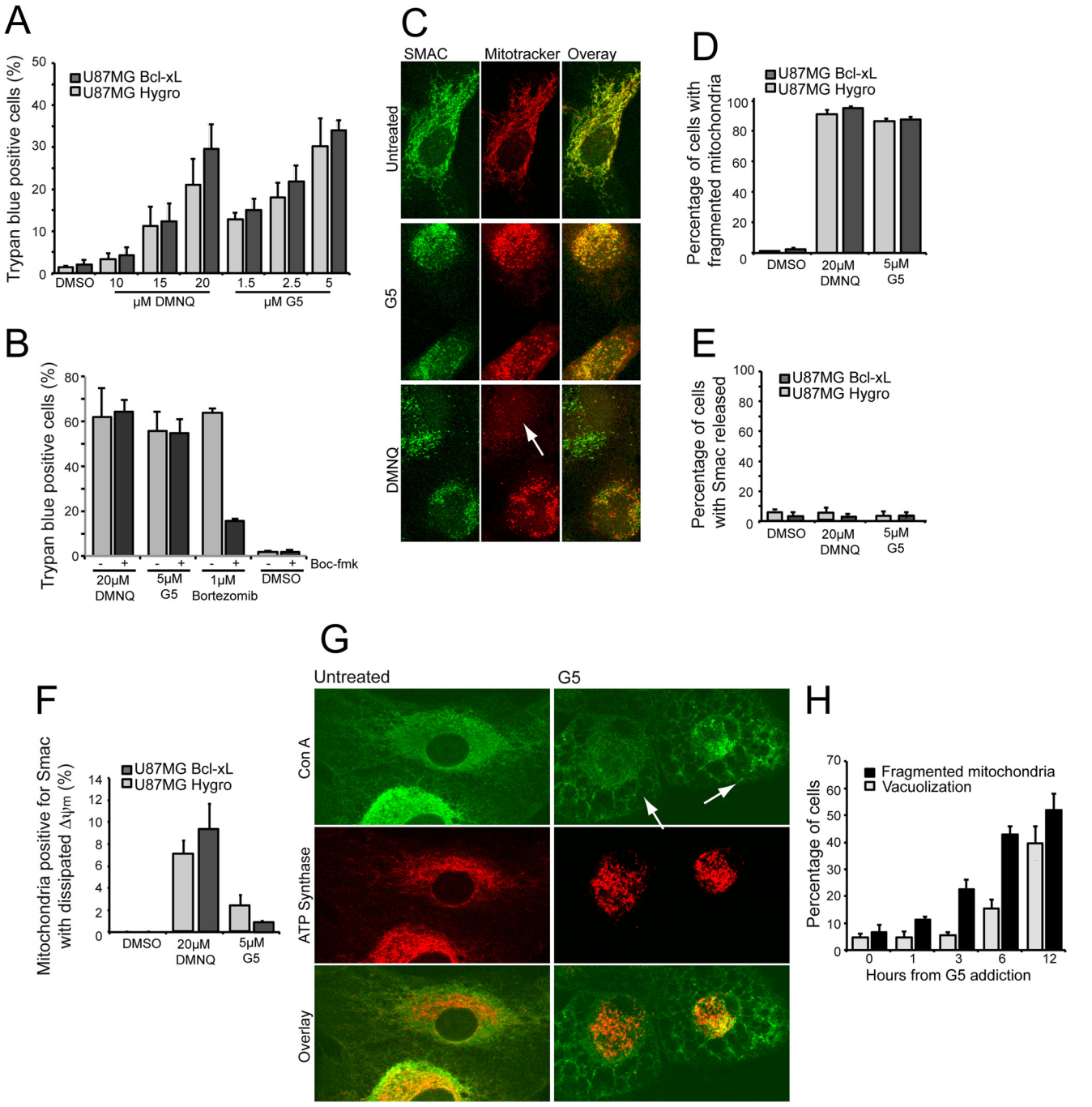

FIGURE 1. **Cell death in U87MG cells in response to G5 or DMNQ treatments.** *A*, U87MG/Hygro and U87MG/Bcl-xL cells were treated with the indicated concentrations for 24 h, and the appearance of cell death was scored by trypan blue staining. *Columns*, mean ($n = 3$); *bars*, S.D. *B*, U87MG/Bcl-xL cells were pretreated for 2 h with 50 μM pan caspase inhibitor Boc-fmk, then 5 μM G5, 20 μM DMNQ, and 1 μM bortezomib were added for 36 h. The appearance of cell death was scored by trypan blue staining. *Columns*, mean ($n = 3$); *bars*, S.D. *C*, U87MG/Bcl-xL cells were treated with G5 or DMNQ for 16 h, and MitoTracker Red was added to the medium 1 h before fixing. Immunofluorescence was performed to visualize Smac subcellular localization and mitochondrial morphology. Cells were analyzed at confocal microscopy. *Arrows* point to cells with evident alterations in $\Delta\psi$m as depicted by reduced MitoTracker Red staining. *D*, quantitative analysis of mitochondrial morphology in U87MG/Bcl-xL and U87MG/Hygro cells treated as indicated in *C*. MitoTracker staining was used to score mitochondrial fragmentation. *E*, quantitative analysis of Smac localization in U87MG/Bcl-xL and U87MG/Hygro cells treated as indicated in *C*. After immunofluorescence 300 cells were classified for each treatment. *F*, quantitative analysis of Smac localization and MitoTracker staining in U87MG/Bcl-xL and U87MG/Hygro cells were treated as indicated in *C*. *G*, U87MG/Bcl-xL cells were treated with G5 5 μM for 12 h. Immunofluorescence analysis was performed to visualize cytosolic vacuolization using concanavalin A (*ConA*), a lectin that stains the endoplasmic reticulum, and mitochondria morphology using anti-ATP synthase antibodies. The *arrows* point to cells with evident cytoplasmic vacuolization. *H*, time course analysis of changes observed, as exemplified in *G* after treatment of U87MG/Bcl-xL cells with G5.

(10%) presented intact mitochondrial outer membrane but decreased MitoTracker staining, thus indicating that $\Delta_{\psi m}$ collapse occurs before mitochondrial outer membrane permeabilization (Fig. 1*F*).

Cytoplasmic vacuolization, as a consequence of endoplasmic reticulum stress, occurs in response to the engagement of the unfolded response by UPS inhibitors (24). As shown in Fig. 1*G*, glioma cells incubated with G5 exhibit cytoplasmic vacuoliza-

tion. However, when a time course analysis was performed, it was evident that mitochondrial fragmentation precedes cytoplasmic vacuolization (Fig. 1*H*). In conclusion, mitochondrial fragmentation is an early event during cell death induced either by G5 or DMNQ treatment.

G5 and DMNQ Activate Distinct Necrotic Pathways—To elucidate the contribution of mitochondrial fragmentation to G5- and DMNQ-induced necrosis, cells were treated with the Drp1 inhibitor Mdivi-1 (25). Mdivi-1 attenuated necrosis only in response to DMNQ (Fig. 2*A*). To confirm this result we generated U87MG/Bcl-xL cells expressing a dominant negative mutant (K38A) of Drp1 (Fig. 2*B*). Treatment with G5 or with DMNQ of Drp1-K38A-overexpressing cells confirmed the result obtained with the Drp1 inhibitor. The dependence from Drp1 activity to fully elicit necrosis was observed only in the case of DMNQ treatment (Fig. 2*C*).

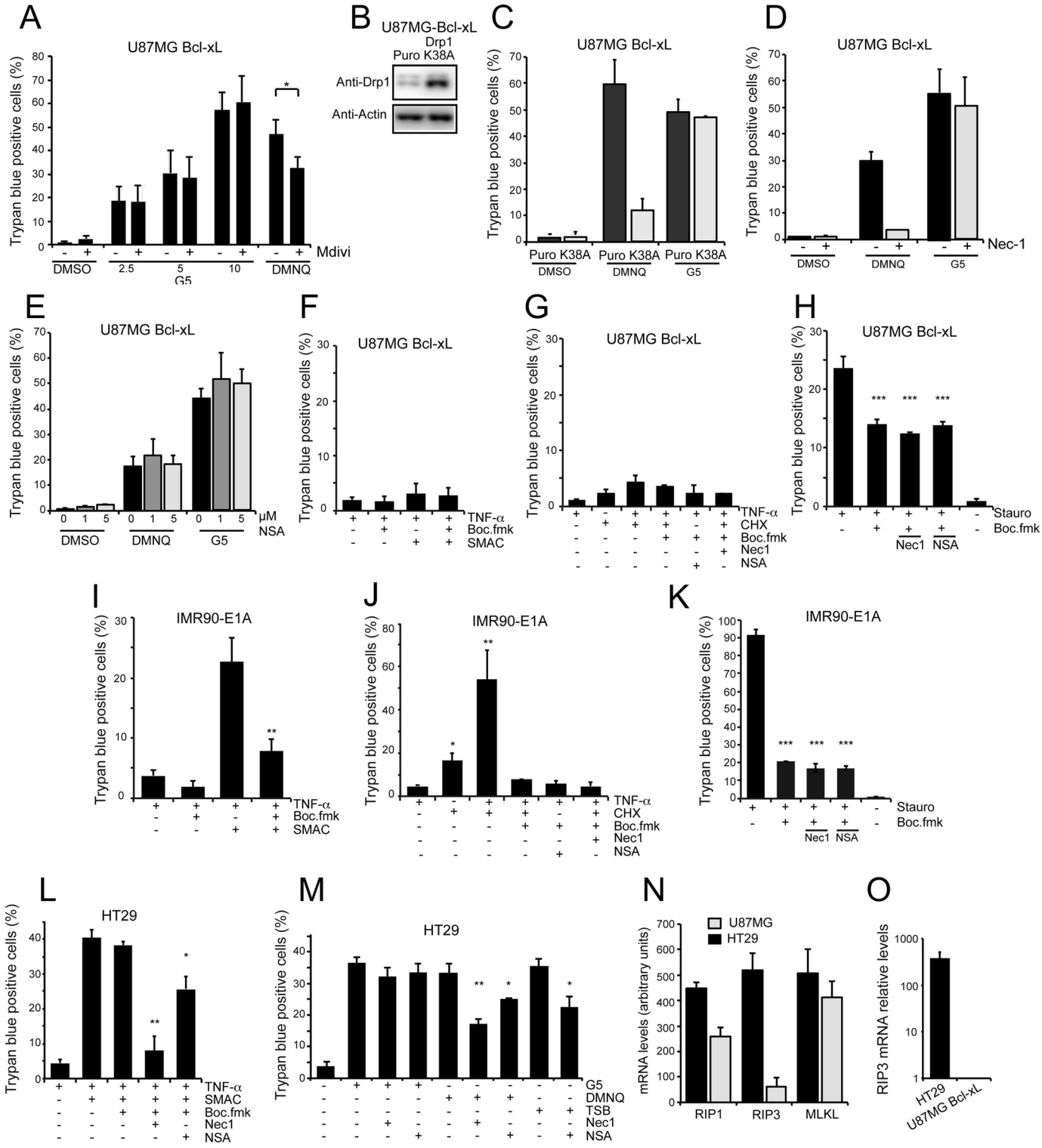

To further prove that necrosis elicited by DMNQ or G5 engages two distinct pathways, we evaluated the contribution of RIP1 by treating cells with the specific inhibitor Nec-1 (9). Cell death was efficiently rescued by Nec-1 only when elicited by DMNQ (Fig. 2*D*). These results demonstrate that two distinct necrotic pathways are activated by DMNQ and G5.

We also investigated the ability of NSA, a MLKL inhibitor that blocks necrosis downstream of RIP3 activation (4), to differentially influence G5- and DMNQ-induced necrosis. Inhibition of MLKL did not suppress the appearance of cell death in response to G5 and, surprisingly, in DMNQ-treated cells as well (Fig. 2*E*). To prove inhibitor efficiency, we treated U87MG/Bcl-xL cells with a classic necroptotic stimulus: the combination TNF-α, Smac mimetic (26), and Boc-fmk, as caspase inhibitor). U87MG cells were unresponsive to the TNF-α, Smac mimetic, and Boc-fmk combination (Fig. 2*F*). We also used cyclohexamide instead of Smac in the combination (TNF-α, cyclohexamide, Boc-fmk). Here again cell death was undetectable (Fig. 2*G*). Finally we used staurosporine, a recently suggested necroptotic trigger (27). Staurosporine induced both apoptosis and necrosis in U87MG/Bcl-xL cells (Fig. 2*H*); however, this necrotic response was unaffected by RIP1 and MLKL inhibition. When the same necrotic triggers were evaluated in IMR90-E1A cells, the vast majority of the cells died by apoptosis, as proved by the effectiveness of the caspase inhibitor (Fig. 2, *I–K*). We also examined colon cancer HT29 cells, commonly utilized for necroptotic experiments. These cells died by necroptosis in response to the TNF-α, Smac mimetic, and Boc-fmk combination. Nec-1 efficiently abrogated this cell death, and NSA was active, although less potent compared with Nec-1 (Fig. 2*L*). These results prove that HT29 cells can die through necroptosis and that the two inhibitors are valuable. When we analyzed G5- and DMNQ-induced death in HT29 cells, similarly to U87MG cells the two drugs exhibited differential susceptibility to RIP1 and MLKL inhibition. G5-induced cell death was unaffected, whereas DMNQ was partially counteracted by the two inhibitors, with Nec-1 showing a stronger effect (Fig. 2*M*). Overall these results further confirm the existence of different necrotic responses.

Finally, we discovered that the divergent responsiveness of HT29 and U87MG cells to necroptotic stimuli and the different responsiveness to MLKL inhibition, in the case of DMNQ-induced necrosis, could be explained by the differential expression of RIP3. In fact, when we interrogated public available gene expression profiles from U87MG and HT29 cells for necroptotic gene mRNA levels (Fig. 2*N*), RIP3 mRNA was clearly reduced in U87MG compared with HT29 cells. Quantitative real-time-PCR experiments proved the dramatic reduction ($\sim$400 times respect to HT29 cells) of RIP3 mRNA in U87MG cells (Fig. 2*O*).

Cellular Responses to G5 Treatment—To gain insight into the necrotic pathway elicited by G5, we decided to monitor the activation of signaling pathways transducing stress and prosurvival signals (28) in G5-treated cells. We evaluated activations of ERKs, p38, JUNK, and Akt. ERKs and p38 but not JUNK were transiently activated in response to G5. However, these activations were anticipated without mirroring the appearance of necrosis (Fig. 3*A*).

When the status of Akt activation was evaluated, it emerged that the kinetic of dephosphorylation of serine 473 and also of threonine 308 (after a transient up-regulation) was paired to the appearance of necrosis (Fig. 2*E*). This result suggests that inhibition of Akt could be linked to G5-induced necrosis.

PP2A can dephosphorylate and inactivate Akt (29, 30). Hence, we monitored PP2A subunit levels in cells treated with G5. Levels of PP2Ac catalytic subunit were increased until 3 h from G5 treatment with a drop at 6 h, after the advent of necrosis. By contrast levels of the scaffold subunit A (PR65) were unaffected. Having discovered an increase of the PP2Ac subunit, we next evaluated whether PP2A enzymatic activity was augmented after G5 treatment, thus explaining Akt dephos-

FIGURE 2. **DMNQ and G5 trigger distinct necrotic types of cell death.** *A*, U87MG/Bcl-xL cells were pretreated with the Drp1 inhibitor Mdivi-1 (50 μM) for 1 h. Next, G5 (indicated concentrations) and DMNQ 30 μM were added for 24 h. The appearance of cell death was scored by trypan blue staining. Data are presented as the mean $\pm$ S.D.; $n = 4$. *B*, immunoblot analysis of U87MG/Bcl-xL cells expressing the Drp1 mutant K38A or Puro gene. Cellular lysates were generated, and an immunoblot analysis performed as indicated. *C*, U87MG/Bcl-xL/Drp1K38A and U87MG/Bcl-xL/Hygro control cells were treated with 5 μM G5 and DMNQ 30 μM for 24 h. The appearance of cell death was scored by trypan blue staining. Data are presented as the mean $\pm$ S.D.; $n = 3$. *D*, U87MG/Bcl-xL cells were pretreated with the RIP1 inhibitor Nec-1 (10 μM) for 1 h. Next, 5 μM G5 and DMNQ 30 μM were added for 24 h. The appearance of cell death was scored by trypan blue staining. Data are presented as the mean $\pm$ S.D.; $n = 3$. *E*, U87MG/Bcl-xL cells were pretreated with the MLKL inhibitor NSA at the indicated concentrations for 1 h. Next, 5 μM G5 and DMNQ 30 μM were added for 24 h. The appearance of cell death was scored by trypan blue staining. Data are presented as the mean $\pm$ S.D.; $n = 3$. *F*, U87MG/Bcl-xL cells were subjected to the indicated treatments for 48 h. Concentrations used were TNF-α (50 ng/ml), Smac mimetic (100 nM), Boc-fmk (50 μM). The appearance of cell death was scored by trypan blue staining. Data are presented as the mean $\pm$ S.D.; $n = 3$. *G*, U87MG/Bcl-xL cells were subjected to the indicated treatments for 36 h. Concentrations used were TNF-α (50 ng/ml), cyclohexamide (*CHX*; 10 μg/ml), Boc-fmk (50 μM), Nec-1 (10 μM), NSA (5 μM). Appearance of cell death was scored by trypan blue staining. Data are presented as the mean $\pm$ S.D.; $n = 3$. *H*, U87MG/Bcl-xL cells were subjected to the indicated treatments for 48 h. Concentrations used staurosporine (5 μM), Boc-fmk (50 μM), Nec-1 (10 μM), and NSA (2 μM). The appearance of cell death was scored by trypan blue staining. Data are presented as the mean $\pm$ S.D.; $n = 3$. *I*, IMR90-E1A cells were subjected to the indicated treatments for 36 h. Concentrations used were TNF-α (50 ng/ml), Smac mimetic (100 nM), and Boc-fmk (50 μM). The appearance of cell death was scored by trypan blue staining. Data are presented as the mean $\pm$ S.D.; $n = 3$. *J*, IMR90-E1A cells were subjected to the indicated treatments for 36 h. Concentrations used were TNF-α (50 ng/ml), cyclohexamide (10 μg/ml), Boc-fmk (50 μM), Nec-1 (10 μM), and NSA (5 μM). The appearance of cell death was scored by trypan blue staining. Data are presented as the mean $\pm$ S.D.; $n = 3$. *K*, U87MG/Bcl-xL cells were subjected to the indicated treatments for 36 h. Concentrations used were staurosporine (1 μM), Boc-fmk (50 μM), Nec-1 (10 μM), and NSA (5 μM). The appearance of cell death was scored by trypan blue staining. Data are presented as the mean $\pm$ S.D.; $n = 3$. *L*, HT29 cells were subjected to the indicated treatments for 36 h. Concentrations used were TNF-α (20 ng/ml), Smac mimetic (100 nM), Boc-fmk (50 μM), Nec-1 (10 μM), and NSA (2 μM). The appearance of cell death was scored by trypan blue staining. Data are presented as the mean $\pm$ S.D.; $n = 3$. *M*, HT29 cells were subjected to the indicated treatments for 36 h. Concentrations used were TNF-α (20 ng/ml), Smac mimetic (100 nM), Boc-fmk (50 μM), G5 (5 μM), DMNQ (30 μM), Nec-1 (10 μM), and NSA (2 μM). The appearance of cell death was scored by trypan blue staining. Data are presented as the mean $\pm$ S.D.; $n = 3$. *N*, mRNA expression levels of RIP1, RIP3, and MLKL in HT29 and U87MG cell lines. Data were derived from public available microarray experiments (GSE48433, GSE23806, GSE14889, and GSE9171). Values are the average of two array chips for U87MG and three for HT29 cells. *Errors bars* represent S.D. *O*, mRNA expression level of RIP3 was measured in U87MG- and HT29-expressing cells using quantitative real-time-PCR. mRNA level was relative to U87MG cells. Values are shown in a logarithmic scale, Data are presented as the mean $\pm$ S.D.; $n = 3$.

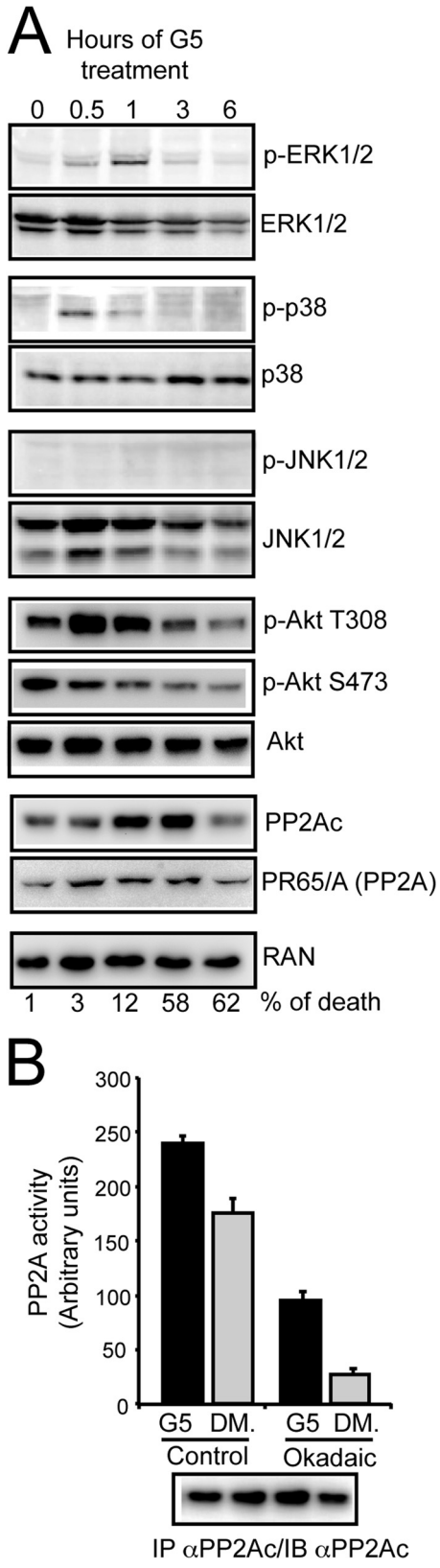

FIGURE 3. **Multiple signaling pathways are engaged after G5 treatment.** *A*, U87MG/Bcl-xL cells were treated with 10 μM G5 for the indicated times. Cellular lysates were generated, and immunoblots were performed with the indicated antibodies. In parallel cell death was scored by trypan blue staining at the same time points, and percentages are represented at the *bottom*. *B*, immunoprecipitation (*IP*) of PP2Ac and fluorimetric assay using DiFMUP substrate. U87MG/Bcl-xL cells were treated with 10 μM G5 or DMSO (*DM*) for 1 h before immunoprecipitation. As the control, immunocomplexes were preincubated with okadaic acid as indicated under "Experimental Procedures." Immunocomplexes were next resolved in SDS/PAGE electrophoresis and immunoblotted to verify the amount of PP2Ac. Data are presented as the mean ± S.D.; $n = 2$.

phorylation and inactivation. Fig. 3*B* illustrates that PP2A phosphatase activity is augmented in cells treated with G5.

Differential Requirements of PP2Ac during Necrotic Death Induced by G5 and DMNQ—To evaluate the contribution of PP2A to G5-induced necrosis, we silenced the expression of the catalytic subunit and next incubated U87MG/Bcl-xL cells with G5 or DMNQ. Down-regulation of PP2Ac impacted both necrotic responses, although with opposite effects (Fig. 4*A*). PP2Ac is required for necrosis in response to G5, but it counteracts necrosis in response to DMNQ. This evidence further strengthens the hypothesis that cells can engage multiple necrotic pathways.

The impact of PP2A in G5-induced necrosis was also evident at the level of mitochondrial fragmentation (Fig. 4*B*). In cells with reduced PP2Ac expression, mitochondria fragmentation is much less pronounced. To confirm the role of PP2A we used another siRNA that targets a different region of PP2Ac. Again, down-regulation of PP2Ac limited necrosis in response to G5 and favored necrosis in response to DMNQ (Fig. 4*C*).

The impact of PP2A on G5-induced necrosis could be related to the status of Akt activation; hence, we evaluated Akt phosphorylation in cells silenced for PP2Ac and treated with G5 for 1 h. Fig. 4*D* and the quantitative analysis in Fig. 4*E* evidence that phosphorylation at threonine 308 was higher after G5 treatment in PP2Ac-silenced cells.

In addition to its well established anti-apoptotic role, Akt has been reported to counteract some kinds of necrotic death (31, 32). Hence, we explored whether the pro-necrotic role of PP2A in G5-treated cells could be explicated through the inhibition of Akt activity. First, by using the PI3K inhibitor LY, we observed that suppression of the PI3K-Akt axis was insufficient for triggering the death of U87MG/Bcl-xL cells (Fig. 4, *F* and *G*). Second, G5-induced necrosis was unaffected by the overexpression of a constitutive active form of Akt (Fig. 4, *H* and *I*). In summary, although Akt activity is down-regulated by G5 treatment and PP2A contributes to this modulation, this kinase does not play a major role during G5-induced necrotic death.

The contribution of PP2A to G5-induced necrosis was confirmed in U-118MG cells, another glioblastoma cell line (Fig. 4*J*). By contrast, in a different apoptosis-resistant cell line represented by human fibroblasts expressing E1A and Bcl2 oncogenes and a catalytic inactive dominant negative mutant of Caspase-9 (19), PP2A was dispensable (Fig. 4*K*). Not surprisingly, as for other cellular processes under PP2A influence, in particular the regulation of the RAS/RAF/MAPK pathway, the outcome is dependent on the genotype (33).

Necrosis Promotes the Cytoplasmic Accumulation of PP2Ac—To further characterize PP2Ac functions during G5-induced necrosis, we analyzed its subcellular localization in comparison with HMGB1, a well known necrotic marker, which translocates from the nucleus into the cytoplasm in response to necrosis (34, 35). In untreated cells PP2Ac evidences a nuclear or a

pan (both nuclear and cytoplasmic) localization (Fig. 5*A*), as quantified in Fig. 5*B*. During G5-induced necrosis, cells presenting an exclusively cytoplasmic localization of PP2Ac emerged (Fig. 5*A*, *arrow*), and cells with prominent nuclear PP2Ac disappeared (Fig. 5*B*). Cells showing accumulation of PP2Ac into the cytosol similarly translocate HMGB1 from the nucleus into the cytoplasm (Fig. 5, *A* and *C*). Interestingly, silencing of PP2Ac reduced the percentage of cells exhibiting cytosolic translocation of HMGB1 in response to G5 treatment (Fig. 5*D*).

The PP2A Substrate Cofilin-1 Influences in a Phosphorylation-dependent Manner Necrosis Induced by G5—PP2A enacts pleiotropic activities in different cellular contexts, which reflects the considerable number of substrates under its supervision (36). On the other side G5 treatment induces profound changes in cell spreading and actin cytoskeleton (18, 22) as exemplified in Fig. 6*A*. Quantitative analysis confirmed the dramatic and rapid alterations in cell morphology upon compound treatment (Fig. 6*B*). We also evaluated the contribution of PP2A to the modification of actin cytoskeleton. Cells were silenced for PP2Ac expression and monitored for changes in adhesion/spreading. As illustrated in Fig. 6*C* and quantified in Fig. 6*D*, down-regulation of PP2Ac promoted reorganization of actin cytoskeleton and augmented cell spreading. Silencing of PP2Ac was also sufficient to constrain in part the reduction

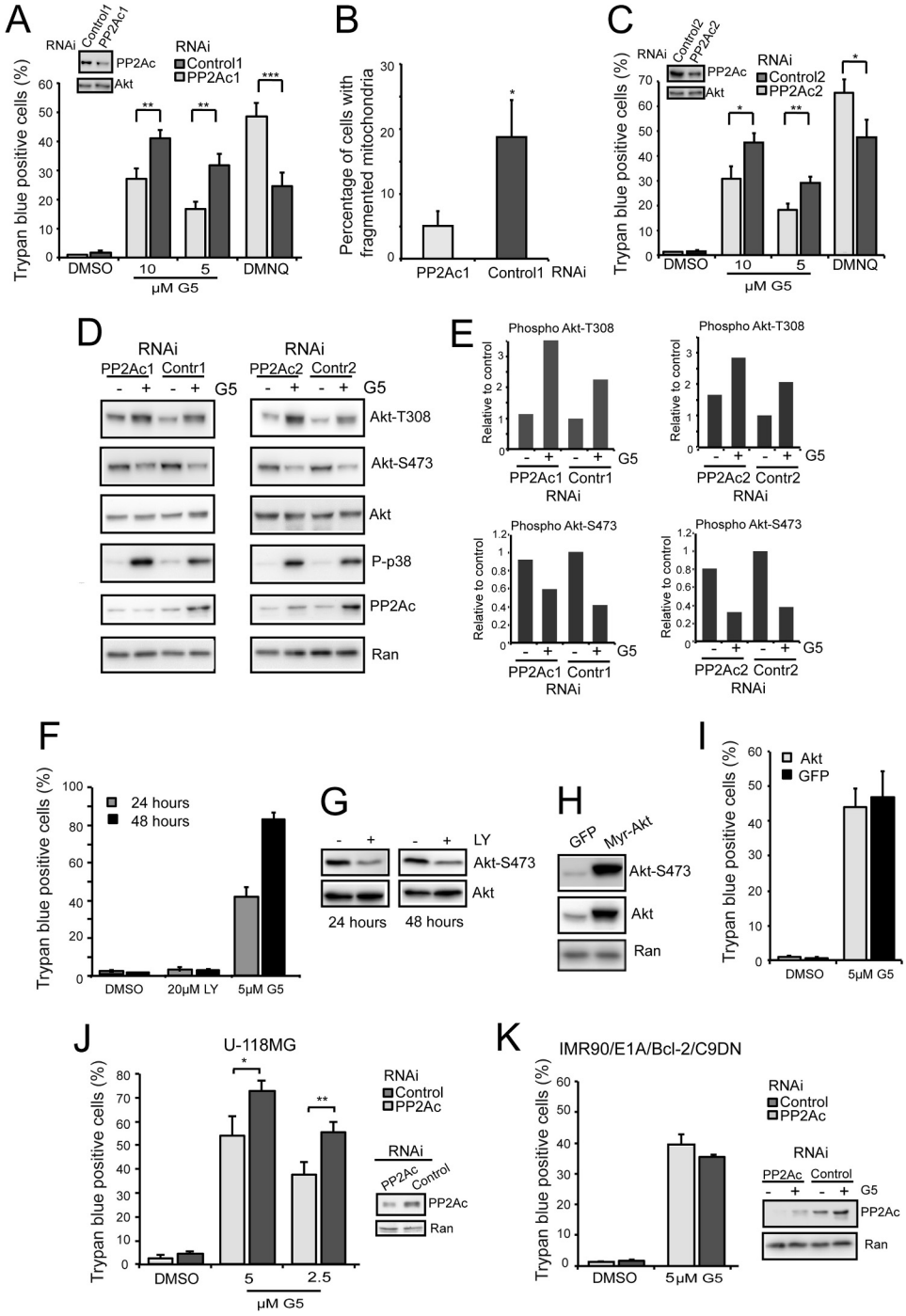

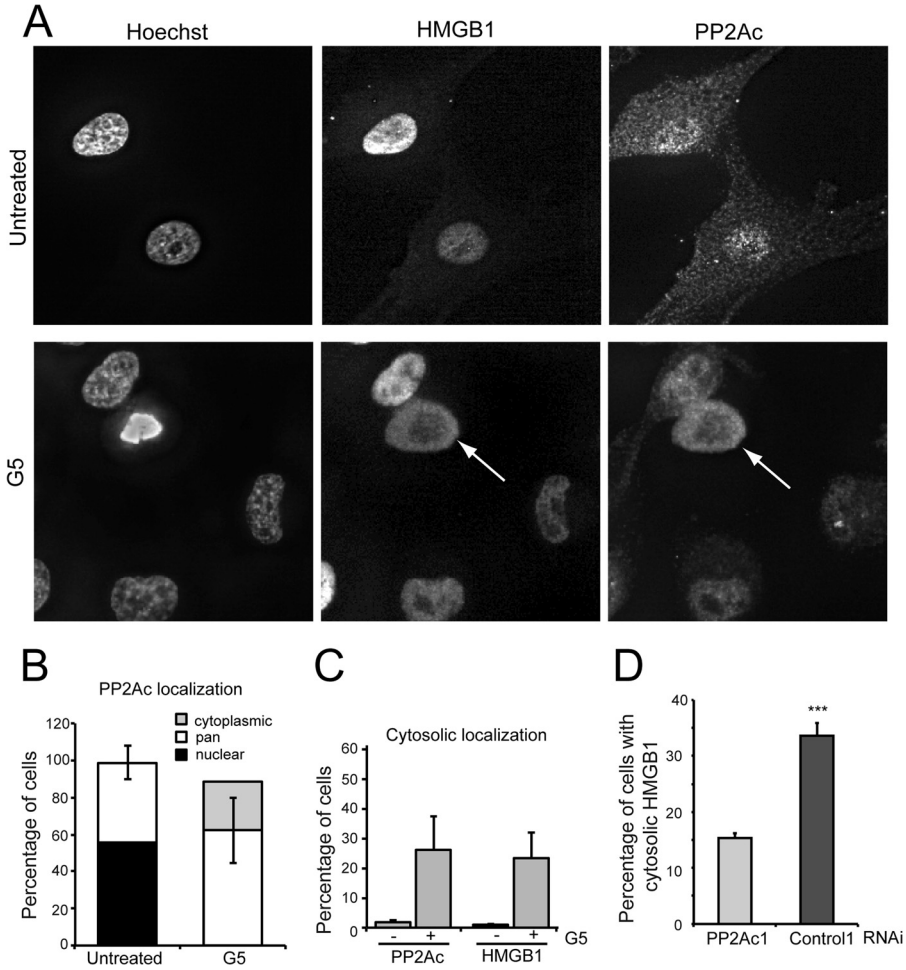

FIGURE 5. **Subcellular relocalization of PP2Ac during G5-induced necrosis.** *A*, U87MG/Bcl-xL cells were treated for 5 h with G5 5 μM. After immunofluorescence, epifluorescence microscopy followed by deconvolution analysis was used to visualize PP2Ac and HMGB1 localization. Hoechst 33258 staining was applied to mark nuclei. The *arrow* points to a cell with evident PP2Ac cytosolic accumulation. *B*, quantitative analysis of PP2Ac and HMGB1 re-localization during G5-induced necrosis. Data are the percentage of cells with pan, cytoplasmic, or nuclear PP2Ac localization in untreated or G5 treated cells. *C*, comparison between cells with cytosolic accumulation of PP2Ac and HMGB1 in G5 treated and untreated cells. *D*, U87MG/Bcl-xL cells transfected with the indicated siRNAs were grown on coverslips for 40 h. Cells were next treated for 18 h with G5 5 μM. HMGB1 localization was scored after immunofluorescence analysis Data are presented as the mean ± S.D.; $n = 3$.

of cell spreading as operated by G5. Furthermore, promoting actin depolymerization using cytochalasin D amplified necrosis in response to G5. The opposite, favoring actin polymerization, using cucurbitacin E restrained G5-induced necrotic death (Fig. 6*E*).

To identify PP2A substrates that could be involved in transducing the necrotic signal to the actin cytoskeleton, we focused our attention on regulators of microfilament dynamics. Cofilin-1, an actin-binding protein with severing activity toward actin filaments, is a PP2A substrate (37, 38). Activation of Cofi-

FIGURE 4. **PP2A plays a key role in the necrotic response to G5 treatment.** *A*, U87MG/Bcl-xL cells were grown for 40 h in the presence of the indicated siRNAs and next treated for 24 h with G5, 5 or 10 μM and 30 μM DMNQ. The appearance of cell death was scored by trypan blue staining. *Columns*, mean ($n = 3$); *bars*, S.D. Immunoblot analysis was performed to evaluate PP2Ac down-regulation by using the indicated antibodies. *B*, U87MG/Bcl-xL cells, transfected with the indicated siRNAs, were grown on glass coverslips for 40 h. Cells were next treated for 18 h with G5 5 μM. After immunofluorescence with anti-ATP synthase antibodies, confocal microscopy was used to score mitochondrial fragmentation. Data are presented as the mean ± S.D.; $n = 3$. *C*, U87MG/Bcl-xL cells were grown for 40 h in the presence of the indicated siRNAs and next treated for 24 h with G5, 5 or 10 μM and 30 μM DMNQ. The appearance of cell death was scored by trypan blue staining. Data are presented as the mean ± S.D.; $n = 3$. *D*, Akt activation in U87MG/Bcl-xL cells treated with G5 and silenced for PP2Ac. Cells were silenced for 48 h and next treated with 10 μM G5 for 1 h. Cellular lysates were generated and probed with the indicated antibodies. *E*, quantitative densitometric analysis of immunoblots. Data are presented as the mean of two experiments. *F*, U87MG/Bcl-xL cells were treated with the indicated concentrations of LY or G5 for 24 and 48 h. The appearance of cell death was scored by trypan blue staining. Data are presented as mean ± S.D.; $n = 3$. *G*, immunoblot analysis of Akt phosphorylation status upon LY treatment in U87MG/Bcl-xL cells. Cellular lysates were generated and probed with the indicated antibodies. *H*, characterization of U87MG expressing myristoylated-Akt (*Myr-Akt*), a constitutively active form of Akt. Cellular lysates were generated and probed with the indicated antibodies. *I*, U87MG cells overexpressing Myr-Akt or GFP were generated and next treated with G5 5 μM for 24 h. The appearance of cell death was scored by trypan blue staining. Data are presented as the mean ± S.D.; $n = 3$. *J*, U-118MG cells were grown for 36 h in the presence of the indicated siRNAs and next treated for 24 h with G5, 5 or 2.5 μM. The appearance of cell death was scored by trypan blue staining. Data are presented as the mean ± S.D.; $n = 3$. Immunoblot analysis was performed to evaluate PP2Ac down-regulation by using the indicated antibodies. *K*, IMR90 cells expressing E1A, Bcl2, and Casp9 dominant negative mutant (*C9DN*) were grown for 40 h in the presence of the indicated siRNAs and next treated for 24 h with 5 μM G5. Cell death was scored by trypan blue staining. Data are presented as the mean ± S.D.; $n = 3$. Immunoblot analysis was performed to evaluate PP2Ac down-regulation in cells treated or not with G5 by using the indicated antibodies.

lin-1 actin depolymerizing function relies on the dephosphorylation of a serine residue at position 3 (39, 40). Hence we evaluated the status of Cofilin Ser-3 phosphorylation in response to G5. Fig. 6*F* illustrates that upon G5 treatment Cofilin is rapidly dephosphorylated at Ser-3. Next we evaluated whether PP2A controls this phosphorylation in U87MG cells. In cells silenced

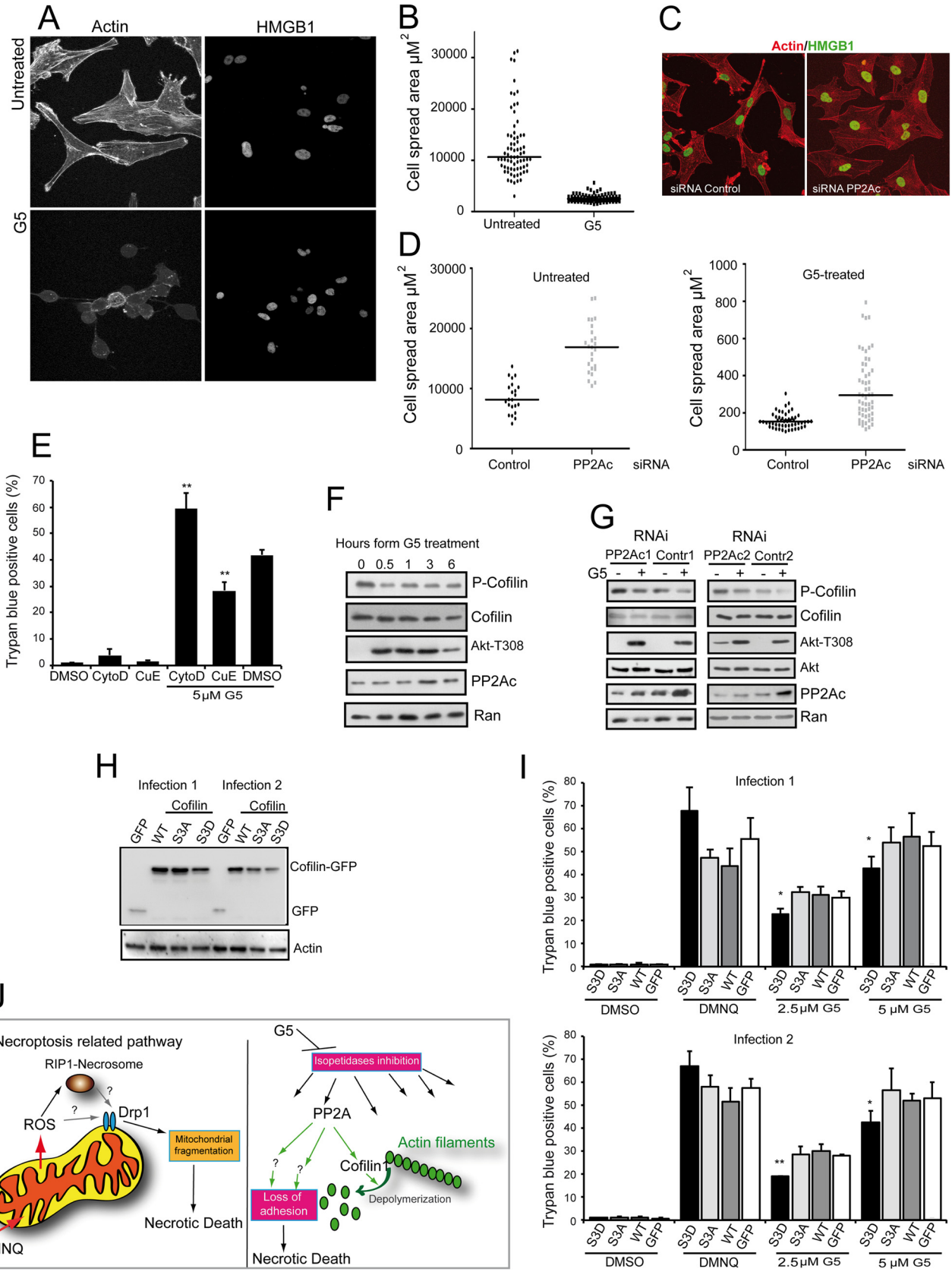

for PP2A, phosphorylation of Ser-3 is augmented, and after G5 treatment dephosphorylation of this residue is less pronounced (Fig. 6*G*). Finally to prove the contribution of Cofilin-1 dephosphorylation to the necrotic death elicited by G5, we generated glioblastoma cells stably expressing Cofilin-1 wt, phosphomimetic S3D substitution, and dephosphomimetic S3A substitution. The immunoblot proved that the different constructs were expressed in U87MG cells (Fig. 6*H*), although the levels of the S3D mutant were in general reduced with respect to the others. When transgenic cells were treated with G5, necrotic cell death was partially but significantly reduced only in cells expressing the phosphomimic S3D mutant that is impaired in the depolymerizating activity (Fig. 6*I*).

DISCUSSION

In this manuscript we have demonstrated the existence of different forms of necrotic death and characterized a new type of regulated necrosis. We demonstrated that DMNQ, a mitochondrial reactive oxygen species inducer, relies on necroptotic components with the involvement of the RIP1, Drp1, and mitochondrial fragmentation, whereas G5, although promoting mitochondrial fragmentation, works independently from this pathway. We have demonstrated that PP2A and its substrate Cofilin-1 influence G5-induced necrosis.

Although the involvement of Drp1 in classical necroptosis is debated (11, 12), our observations indicate an important contribution of the GTPase during DMNQ-induced necrosis (Fig. 6*J*). This contribution could reflect the specific generation of mitochondrial stress as recently proposed (41–43). Peculiarities in the DMNQ-induced necrosis emerged also after comparing HT29 and U87MG cells. Although in the colon cancer cells DMNQ requires RIP1 and MLKL, in U87MG cells, which express extremely low levels of RIP3, it can induce necrosis without the apparent involvement of MLKL (12). Further studies are necessary to clarify these points.

G5 belongs to a family of small compounds that share the same pharmacophore capable of reacting with cellular cysteines (21, 44, 45). These molecules promote accumulation of polyubiquitinated proteins but through different mechanisms with respect to inhibitors of the proteasome catalytic core (21, 46). Recently it has been shown that a G5-like compound reacts with Cys-88 of RPN13, a subunit of the 19 S proteasome complex involved in recognizing K-48 polyubiquitinated peptides (44). This reaction impacts on protein degradation and explains the accumulation of the catalytic subunit of Ser/Thr phosphatase PP2A, which is under proteasomal control (47). G5 does not simply stabilize PP2Ac but also augments its catalytic activity.

PP2A up-regulation can also take place in response to bortezomib. However bortezomib is much less potent as necrotic inducer compared with G5 (18, 22). This observation suggests that in glioblastoma cells treated with G5 additional stresses, perturbations are present that require the activity of PP2A for an efficient death. In fact *in vitro* studies have highlighted that nonselective isopeptidase inhibitors (NS-II) can inhibit different deubiquitinases (DUBs) and also SUMO (small ubiquitin-like modifier) proteases (46), all isopeptidases characterized by the presence of a cysteine in the catalytic core.

Our results demonstrate that PP2A can act as necrotic regulator showing opposite outcomes in response to different insults. PP2A is pro-necrotic in the case of G5 but anti-necrotic in the case of DMNQ. In agreement with our result, a protective role of PP2A was demonstrated upon H_2O_2 treatment (48). Diverse outcomes are not surprising for PP2A. Different signaling pathways operating in a specific cellular context and the blend of regulative subunits, which constitute the active enzyme, could explain the opposite influences of PP2A on necrosis (36). In fact, PP2A are holoenzymes composed of a scaffolding/structural subunit, a catalytic subunit, and a variable regulatory subunit with several family members (49).

We also observed a translocation of nuclear PP2Ac into the cytoplasm early during necrosis, which is timely coupled to the nuclear release HMGB1, a well known necrotic marker (34, 35). This phenomenon needs to be further investigated to discern between an indiscriminate release of several nuclear factors and a specific spatial/temporal regulation of PP2Ac localization. Certainly, in addition to the increased activity linked to G5 treatment, enzyme redistribution could also contribute to generate a necrotic specific phosphoproteome.

Akt, an important PP2A substrate, in which phosphorylation is modulated by G5 treatment, does not play a key role during this necrotic response. Instead, the most outstanding effect of PP2Ac down-regulation in U87MG glioblastoma cells was the reorganization of actin cytoskeleton and of cell adhesion. PP2A down-regulation increased the number of stress fibers and the spreading area and counteracted the dramatic changes of actin architecture and adhesion observed in cells treated with isopep-

FIGURE 6. **The role of actin cytoskeleton in the necrotic death elicited by G5.** *A*, confocal pictures of U87MG/Bcl-xL cells treated or not for 5 h with G5 5 μM. Immunofluorescence analysis was performed to visualize HMGB1 subcellular localization, and TRITC-phalloidin was used to decorate actin filaments. *B*, quantitative analysis of changes in cell adhesion after treatment for 5 h with G5 5 μM. Cell spread area was quantified using MetaMorph. Results shown are from three independent experiments. *C*, confocal pictures of U87MG/Bcl-xL cells transfected with a siRNA against PP2A or control siRNA. Immunofluorescence analysis was performed to visualize HMGB1 subcellular localization (*green*), and TRITC-phalloidin was used to decorate actin filaments (*red*). Images are shown in pseudocolors. *D*, quantitative analysis of changes in cell adhesion after treatment for 5 h with G5 5 μM. Cells were transfected as in *C* and fixed, immunofluorescence analysis was performed, and finally the coverslips were subjected to the quantitative analysis. The cell spread area was quantified using MetaMorph. Results shown are from three independent experiments. *E*, U87MG/Bcl-xL cells were treated with 50 μM cytochalasin D or 50 nM CucE for the 48 h. When used in combination with G5, cell death was scored after 24 h and 1 h of pretreatment before G5 addition was applied. The appearance of cell death was scored by trypan blue staining. Data are presented as the mean ± S.D.; $n = 3$. *F*, U87MG/Bcl-xL cells were treated with 10 μM G5 for the indicated times. Cellular lysates were generated, and immunoblots performed with the indicated antibodies. *G*, U87MG/Bcl-xL cells were silenced for 48 h and next treated with 10 μM G5 for 1 h. Cellular lysates were generated and probed with the indicated antibodies. *H*, immunoblot analysis of U87MG/Bcl-xL cells expressing the cofilin-1 fused to GFP, the S3A or Asp mutants, and the GFP alone as control. Cellular lysates were generated, and immunoblot analysis performed using an anti-GFP antibody. Two different retroviral infections were used. *I*, U87MG/Bcl-xL cells expressing the different transgenes were treated with the indicated concentrations of G5 and DMNQ 30 μM for 24 h. The appearance of cell death was scored by trypan blue staining. Data are presented as the mean ± S.D.; $n = 4$. *J*, summary of the different necrotic pathways engaged by DMNQ and G5. *ROS*, reactive oxygen species.

tidase inhibitors. Furthermore, modulation of the actin cytoskeleton can influence the magnitude of the G5-necrotic response. These results confirm our previous studies on the involvement of the extracellular matrix in the regulation of this necrotic death (18, 22).

Although relationships between PP2A and actin/cytoskeleton have been studied in the past, few substrates influencing the cytoskeleton have been identified. Among them there is Cofilin-1, an actin-binding protein with severing activity toward actin filaments (37). The activation of the actin depolymerizing function of Cofilin-1 relies on the dephosphorylation of a serine residue at position 3 (39, 40, 50). G5 treatment elicited a rapid decrease of Cofilin-1 Ser-3 phosphorylation. The down-regulation of PP2Ac increased Ser-3 phosphorylation, and the concomitant treatment with G5 attenuated the de-phosphorylation/activation of Cofilin with respect to control. Silencing of PP2Ac did not abrogate Cofilin dephosphorylation, thus implying the contribution of additional phosphatases, such as the slingshot (SSH) family of protein phosphatases (39).

The protective effect observed with the Cofilin phosphomimic mutant during G5-induced cell death was partial. Furthermore, cells stably expressing this mutant do not evidence the profound reorganization of actin cytoskeleton and adhesion observed after PP2Ac silencing. This observation indicates that although Cofilin-1 is a player of this necrotic death, additional PP2A substrates must be involved. For example, a contribution of p21-activated kinases (PAKs), well known orchestrators of actin cytoskeleton and PP2A partners, could be hypothesized (51). Additional PP2A targets should be searched among integrins and the effectors of the signaling pathway engaged by the adhesion to the extracellular matrix (38, 52, 53).

In conclusion we have identified new pieces of the necrotic puzzle. It is evident that further studies are necessary to complete the final picture. Definition the complexity of the necrotic response is an important step of the research with possible implications for understanding human diseases characterized by altered rates of cell death but could also represent a rewarding option to overcome apoptotic resistance of cancer cells.

Acknowledgment—We thank Raffaella Picco for helping with the microarray analysis.

REFERENCES

1. Vanlangenakker, N., Vanden Berghe, T., and Vandenabeele, P. (2012) Many stimuli pull the necrotic trigger, an overview. *Cell. Death Differ.* **19,** 75–86
2. Vanden Berghe, T., Linkermann, A., Jouan-Lanhouet, S., Walczak, H., and Vandenabeele, P. (2014) Regulated necrosis: the expanding network of non-apoptotic cell death pathways. *Nat. Rev. Mol. Cell Biol.* **15,** 135–147
3. Laster, S. M., Wood, J. G., and Gooding, L. R. (1988) Tumor necrosis factor can induce both apoptic and necrotic forms of cell lysis. *J. Immunol.* **141,** 2629–2634
4. Sun, L., Wang, H., Wang, Z., He, S., Chen, S., Liao, D., Wang, L., Yan, J., Liu, W., Lei, X., and Wang, X. (2012) Mixed lineage kinase domain-like protein mediates necrosis signaling downstream of RIP3 kinase. *Cell* **148,** 213–227
5. Cho, Y. S., Challa, S., Moquin, D., Genga, R., Ray, T. D., Guildford, M., and Chan, F. K. (2009) Phosphorylation-driven assembly of the RIP1-RIP3 complex regulates programmed necrosis and virus-induced inflammation. *Cell* **137,** 1112–1123
6. Li, J., McQuade, T., Siemer, A. B., Napetschnig, J., Moriwaki, K., Hsiao, Y. S., Damko, E., Moquin, D., Walz, T., McDermott, A., Chan, F. K., and Wu, H. (2012) The RIP1/RIP3 necrosome forms a functional amyloid signaling complex required for programmed necrosis. *Cell* **150,** 339–350
7. Cai, Z., Jitkaew, S., Zhao, J., Chiang, H. C., Choksi, S., Liu, J., Ward, Y., Wu, L. G., and Liu, Z. G. (2014) Plasma membrane translocation of trimerized MLKL protein is required for TNF-induced necroptosis. *Nat. Cell Biol.* **16,** 55–65
8. Moriwaki, K., and Chan, F. K. (2013) RIP3: a molecular switch for necrosis and inflammation. *Genes Dev.* **27,** 1640–1649
9. Degterev, A., Hitomi, J., Germscheid, M., Ch'en, I. L., Korkina, O., Teng, X., Abbott, D., Cuny, G. D., Yuan, C., Wagner, G., Hedrick, S. M., Gerber, S. A., Lugovskoy, A., and Yuan, J. (2008) Identification of RIP1 kinase as a specific cellular target of necrostatins. *Nat. Chem. Biol.* **4,** 313–321
10. Wang, Z., Jiang, H., Chen, S., Du, F., and Wang, X. (2012) The mitochondrial phosphatase PGAM5 functions at the convergence point of multiple necrotic death pathways. *Cell* **148,** 228–243
11. Moujalled, D. M., Cook, W. D., Murphy, J. M., and Vaux, D. L. (2014) Necroptosis induced by RIPK3 requires MLKL but not Drp1. *Cell Death Dis.* **5,** e1086
12. Remijsen, Q., Goossens, V., Grootjans, S., Van den Haute, C., Vanlangenakker, N., Dondelinger, Y., Roelandt, R., Bruggeman, I., Goncalves, A., Bertrand, M. J., Baekelandt, V., Takahashi, N., Berghe, T. V., and Vandenabeele, P. (2014) Depletion of RIPK3 or MLKL blocks TNF-driven necroptosis and switches towards a delayed RIPK1 kinase-dependent apoptosis. *Cell Death Dis.* **5,** e1004
13. Boya, P., and Kroemer, G. (2008) Lysosomal membrane permeabilization in cell death. *Oncogene* **27,** 6434–6451
14. Arnandis, T., Ferrer-Vicens, I., García-Trevijano, E. R., Miralles, V. J., García, C., Torres, L., Viña, J. R., and Zaragozá, R. (2012) Calpains mediate epithelial-cell death during mammary gland involution: mitochondria and lysosomal destabilization. *Cell Death Differ.* **19,** 1536–1548
15. Moubarak, R. S., Yuste, V. J., Artus, C., Bouharrour, A., Greer, P. A., Menissier-de Murcia, J., and Susin, S. A. (2007) Sequential activation of poly(ADP-ribose) polymerase 1, calpains, and Bax is essential in apoptosis-inducing factor-mediated programmed necrosis. *Mol. Cell. Biol.* **27,** 4844–4862
16. Xu, Y., Huang, S., Liu, Z. G., and Han, J. (2006) Poly(ADP-ribose) polymerase-1 signaling to mitochondria in necrotic cell death requires RIP1/TRAF2-mediated JNK1 activation. *J. Biol. Chem.* **281,** 8788–8795
17. Temkin, V., Huang, Q., Liu, H., Osada, H., and Pope, R. M. (2006) Inhibition of ADP/ATP exchange in receptor-interacting protein-mediated necrosis. *Mol. Cell. Biol.* **26,** 2215–2225
18. Foti, C., Florean, C., Pezzutto, A., Roncaglia, P., Tomasella, A., Gustincich, S., and Brancolini, C. (2009) Characterization of caspase-dependent and caspase-independent deaths in glioblastoma cells treated with inhibitors of the ubiquitin-proteasome system. *Mol. Cancer Ther.* **8,** 3140–3150
19. Henderson, C. J., Aleo, E., Fontanini, A., Maestro, R., Paroni, G., and Brancolini, C. (2005) Caspase activation and apoptosis in response to proteasome inhibitors. *Cell Death Differ.* **12,** 1240–1254
20. Wegner, A. M., McConnell, J. L., Blakely, R. D., and Wadzinski, B. E. (2007) An automated fluorescence-based method for continuous assay of PP2A activity. *Methods Mol. Biol.* **365,** 61–69
21. Aleo, E., Henderson, C. J., Fontanini, A., Solazzo, B., and Brancolini, C. (2006) Identification of new compounds that trigger apoptosome-independent caspase activation and apoptosis. *Cancer Res.* **66,** 9235–9244
22. Fontanini, A., Foti, C., Potu, H., Crivellato, E., Maestro, R., Bernardi, P., Demarchi, F., and Brancolini, C. (2009) The isopeptidase inhibitor G5 triggers a caspase-independent necrotic death in cells resistant to apoptosis: a comparative study with the proteasome inhibitor bortezomib. *J. Biol. Chem.* **284,** 8369–8381
23. Tchivilev, I., Madamanchi, N. R., Vendrov, A. E., Niu, X. L., and Runge, M. S. (2008) Identification of a protective role for protein phosphatase 1cγ1 against oxidative stress-induced vascular smooth muscle cell apoptosis. *J. Biol. Chem.* **283,** 22193–22205
24. Mimnaugh, E. G., Xu, W., Vos, M., Yuan, X., Isaacs, J. S., Bisht, K. S., Gius, D., and Neckers, L. (2004) Simultaneous inhibition of hsp 90 and the proteasome promotes protein ubiquitination, causes endoplasmic reticu-

lum-derived cytosolic vacuolization, and enhances antitumor activity. *Mol. Cancer Ther.* **3,** 551–566
25. Cassidy-Stone, A., Chipuk, J. E., Ingerman, E., Song, C., Yoo, C., Kuwana, T., Kurth, M. J., Shaw, J. T., Hinshaw, J. E., Green, D. R., and Nunnari, J. (2008) Chemical inhibition of the mitochondrial division dynamin reveals its role in Bax/Bak-dependent mitochondrial outer membrane permeabilization. *Dev. Cell* **14,** 193–204
26. Lecis, D., Mastrangelo, E., Belvisi, L., Bolognesi, M., Civera, M., Cossu, F., De Cesare, M., Delia, D., Drago, C., Manenti, G., Manzoni, L., Milani, M., Moroni, E., Perego, P., Potenza, D., Rizzo, V., Scavullo, C., Scolastico, C., Servida, F., Vasile, F., and Seneci, P. (2012) Dimeric Smac mimetics/IAP inhibitors as *in vivo* active pro-apoptotic agents. Part II: structural and biological characterization. *Bioorg. Med. Chem.* **20,** 6709–6723
27. Dunai, Z. A., Imre, G., Barna, G., Korcsmaros, T., Petak, I., Bauer, P. I., and Mihalik, R. (2012) Staurosporine induces necroptotic cell death under caspase-compromised conditions in U937 cells. *PLoS ONE* **7,** e41945
28. Kyriakis, J. M., and Avruch, J. (2012) Mammalian MAPK signal transduction pathways activated by stress and inflammation: a 10-year update. *Physiol. Rev.* **92,** 689–737
29. Kuo, Y. C., Huang, K. Y., Yang, C. H., Yang, Y. S., Lee, W. Y., and Chiang, C. W. (2008) Regulation of phosphorylation of Thr-308 of Akt, cell proliferation, and survival by the B55α regulatory subunit targeting of the protein phosphatase 2A holoenzyme to Akt. *J. Biol. Chem.* **283,** 1882–1892
30. Li, G., Ji, X. D., Gao, H., Zhao, J. S., Xu, J. F., Sun, Z. J., Deng, Y. Z., Shi, S., Feng, Y. X., Zhu, Y. Q., Wang, T., Li, J. J., and Xie, D. (2012) EphB3 suppresses non-small-cell lung cancer metastasis via a PP2A/RACK1/Akt signalling complex. *Nat. Commun.* **3,** 667
31. Mochizuki, T., Asai, A., Saito, N., Tanaka, S., Katagiri, H., Asano, T., Nakane, M., Tamura, A., Kuchino, Y., Kitanaka, C., and Kirino, T. (2002) Akt protein kinase inhibits non-apoptotic programmed cell death induced by ceramide. *J. Biol. Chem.* **277,** 2790–2797
32. Liu, Q., Qiu, J., Liang, M., Golinski, J., van Leyen, K., Jung, J. E., You, Z., Lo, E. H., Degterev, A., and Whalen, M. J. (2014) Akt and mTOR mediate programmed necrosis in neurons. *Cell Death Dis.* **5,** e1084
33. Eichhorn, P. J., Creyghton, M. P., and Bernards, R. (2009) Protein phosphatase 2A regulatory subunits and cancer. *Biochim. Biophys Acta* **1795,** 1–15
34. Scaffidi, P., Misteli, T., and Bianchi, M. E. (2002) Release of chromatin protein HMGB1 by necrotic cells triggers inflammation. *Nature* **418,** 191–195
35. Ditsworth, D., Zong, W. X., and Thompson, C. B. (2007) Activation of poly(ADP)-ribose polymerase (PARP-1) induces release of the pro-inflammatory mediator HMGB1 from the nucleus. *J. Biol. Chem.* **282,** 17845–17854
36. Seshacharyulu, P., Pandey, P., Datta, K., and Batra, S. K. (2013) Phosphatase: PP2A structural importance, regulation and its aberrant expression in cancer. *Cancer Lett.* **335,** 9–18
37. Ambach, A., Saunus, J., Konstandin, M., Wesselborg, S., Meuer, S. C., and Samstag, Y. (2000) The serine phosphatases PP1 and PP2A associate with and activate the actin-binding protein cofilin in human T lymphocytes. *Eur. J. Immunol.* **30,** 3422–3431
38. Oleinik, N. V., Krupenko, N. I., and Krupenko, S. A. (2010) ALDH1L1 inhibits cell motility via dephosphorylation of cofilin by PP1 and PP2A. *Oncogene* **29,** 6233–6244
39. Niwa, R., Nagata-Ohashi, K., Takeichi, M., Mizuno, K., and Uemura, T. (2002) Control of actin reorganization by Slingshot, a family of phosphatases that dephosphorylate ADF/cofilin. *Cell* **108,** 233–246
40. Blangy, A., Touaitahuata, H., Cres, G., and Pawlak, G. (2012) Cofilin activation during podosome belt formation in osteoclasts. *PLoS ONE* **7,** e45909
41. Guo, X., Sesaki, H., and Qi, X. (2014) Protein phosphatase 2A regulatory subunits and cancer. *Biochem. J.* **461,** 137–146
42. Kim, J. E., Ryu, H. J., Kim, M. J., and Kang, T. C. (2014) LIM kinase-2 induces programmed necrotic neuronal death via dysfunction of DRP1-mediated mitochondrial fission. *Cell Death Differ.* **21,** 1036–1049
43. Su, Y. C., Chiu, H. W., Hung, J. C., and Hong, J. R. (2014) β-Nodavirus B2 protein induces hydrogen peroxide production, leading to Drp1-recruited mitochondrial fragmentation and cell death via mitochondrial targeting. *Apoptosis*, in press
44. Anchoori, R. K., Karanam, B., Peng, S., Wang, J. W., Jiang, R., Tanno, T., Orlowski, R. Z., Matsui, W., Zhao, M., Rudek, M. A., Hung, C. F., Chen, X., Walters, K. J., and Roden, R. B. (2013) A bis-benzylidine piperidone targeting proteasome ubiquitin receptor RPN13/ADRM1 as a therapy for cancer. *Cancer Cell* **24,** 791–805
45. Mullally, J. E., and Fitzpatrick, F. A. (2002) Pharmacophore model for novel inhibitors of ubiquitin isopeptidases that induce p53-independent cell death. *Mol. Pharmacol.* **62,** 351–358
46. Nicholson, B., Leach, C. A., Goldenberg, S. J., Francis, D. M., Kodrasov, M. P., Tian, X., Shanks, J., Sterner, D. E., Bernal, A., Mattern, M. R., Wilkinson, K. D., and Butt, T. R. (2008) Characterization of ubiquitin and ubiquitin-like-protein isopeptidase activities. *Protein Sci.* **17,** 1035–1043
47. LeNoue-Newton, M., Watkins, G. R., Zou, P., Germane, K. L., McCorvey, L. R., Wadzinski, B. E., and Spiller, B. W. (2011) The E3 ubiquitin ligase- and protein phosphatase 2A (PP2A)-binding domains of the α4 protein are both required for α4 to inhibit PP2A degradation. *J. Biol. Chem.* **286,** 17665–17671
48. Chen, L., Liu, L., Yin, J., Luo, Y., and Huang, S. (2009) Hydrogen peroxide-induced neuronal apoptosis is associated with inhibition of protein phosphatase 2A and 5, leading to activation of MAPK pathway. *Int. J. Biochem. Cell Biol.* **41,** 1284–1295
49. Janssens, V., and Goris, J. (2001) Protein phosphatase 2A: a highly regulated family of serine/threonine phosphatases implicated in cell growth and signalling. *Biochem. J.* **353,** 417–439
50. Moriyama, K., Iida, K., and Yahara, I. (1996) Phosphorylation of Ser-3 of cofilin regulates its essential function on actin. *Genes Cells* **1,** 73–86
51. Westphal, R. S., Coffee, R. L., Jr., Marotta, A., Pelech, S. L., and Wadzinski, B. E. (1999) Identification of kinase-phosphatase signaling modules composed of p70 S6 kinase-protein phosphatase 2A (PP2A) and p21-activated kinase-PP2A. *J. Biol. Chem.* **274,** 687–692
52. Gushiken, F. C., Patel, V., Liu, Y., Pradhan, S., Bergeron, A. L., Peng, Y., and Vijayan, K. V. (2008) Protein phosphatase 2A negatively regulates integrin α(IIb)β3 signaling. *J. Biol. Chem.* **283,** 12862–12869
53. Nho, R. S., and Kahm, J. (2010) β1-Integrin-collagen interaction suppresses FoxO3a by the coordination of Akt and PP2A. *J. Biol. Chem.* **285,** 14195–14209